Bioorganic & Medicinal Chemistry 17 (2009) 3152–3161

Contents lists available at ScienceDirect

Bioorganic & Medicinal Chemistry

journal homepage: www.elsevier.com/locate/bmc

基于结构的Src激酶抑制剂的虚拟筛选

Structure-based virtual screening of Src kinase inhibitors

Kyungik Lee [a,b], Jongwoo Kim [b], Ki-Woong Jeong [c], Ki Won Lee [c], Yeonjoo Lee [b], Ji Yeon Song [b], Maeng Sup Kim [b], Gwan Sun Lee [b], Yangmee Kim [c,*]

[a] Department of Chemistry, Konkuk University, Seoul 143-701, Republic of Korea
[b] Hanmi Research Center, Hanmi Pharmaceutical Co. Ltd, 377-1 Yeongcheon-ri, Dongtan-myeon, Hwaseong, Gyeonggi-do 445-813, Republic of Korea
[c] Department of Bioscience and Biotechnology, Konkuk University, Seoul 143-701, Republic of Korea

ARTICLE INFO

Article history:
Received 26 November 2008
Revised 26 February 2009
Accepted 27 February 2009
Available online 5 March 2009

Keywords:
Src
Kinase
Inhibitor
Virtual screening
Docking
LIGANDFIT
Drug discovery

ABSTRACT

Src is an important target in multiple processes associated with tumor growth and development, including proliferation, neovascularization, and metastasis. In this study, hit identification was performed by virtual screening of commercial and in-house compound libraries. Docking studies for the hits were performed, and scoring functions were used to evaluate the docking results and to rank ligand-binding affinities. Subsequently, hit optimization for potent and selective candidate Src inhibitors was performed through focused library design and docking analyses. Consequently, we report that a novel compound '**43**' with an IC_{50} value of 89 nM, representing (*S*)-*N*-(4-(5-chlorobenzo[*d*][1,3]dioxol-4-ylamino)-7-(2-methoxyethoxy)quinazolin-6-yl)pyrrolidine-2-carboxamide, is highly selective for Src in comparison to EGFR (IC_{50} ratio > 80-fold) and VEGFR-2 (IC_{50} ratio > 110-fold). Compound **43** exerted anti-proliferative effects on Src-expressing PC3 human prostate cancer and A431 human epidermoid carcinoma cells, with calculated IC_{50} values of 1.52 and 0.78 μM, respectively. Moreover, compound **43** (0.1 μM) suppressed the phosphorylation of extracellular signal-regulated kinases and p90 ribosomal S6 kinase, downstream molecules of Src, in a time-dependent manner, in both PC3 and A431 cell lines. The docking structure of compound **43** with Src disclosed that the chlorobenzodioxole moiety and pyrrolidine ring of C-6 quinazoline appeared to fit tightly into the hydrophobic pocket of Src. Additionally, the pyrrolidine NH forms a hydrogen bond with the carboxyl group of Asp348. These results confirm the successful application of virtual screening studies in the lead discovery process, and suggest that our novel compound **43** can be an effective Src inhibitor candidate for further lead optimization.

1. Introduction

The viral Src gene encoded by Rous sarcoma virus (RSV) was the first defined oncogene encoding the first recognized tyrosine kinase.[1] Tyrosine Kinase (TK)-induced phosphorylation of proteins is a fundamental mechanism for the control of cell growth and differentiation. Src kinase is a member of a structurally homologous group of nonreceptor TKs present in the cytoplasm, known as the 'Src family of kinases'.[2] Src participates in several signaling pathways regulating proliferation, differentiation, and migration,[3] and small-molecule inhibitors of this protein are under investigation as potential agents for the treatment of a variety of diseases.[4,5]

It is proposed that inhibitors of Src phosphorylation may impede uncontrolled tumor cell growth, and thus function as novel therapeutic agents for cancer. Specifically, Src activity is elevated in breast, pancreatic, ovarian, esophageal, lung, gastric, colon, and head-and-neck cancers.[6–10] A number of planar heteroaromatic small-molecule inhibitor templates have been exploited to identify novel Src kinase inhibitors. To date, purine, pyrrolopyrimidine, pyridopyrimidine, naphthyridone, quinazoline, and quinoline-based inhibitors have been reported.[11] Among these, Dasatinib (BMS354825; Bristol Meyers Squibb Oncology),[12] AZD-0530 (AstraZeneca)[13], and Bosutinib (SKI-606; Wyeth Research),[14] have reached Phase 1 or 2 clinical trials (Fig. 1). These small-molecule inhibitors have similar structures derived from 'flat' heterocyclic cores, and specifically inactivate the ATP-binding site of Src family kinases. A dual Src/Abl inhibitor, AZD-0530, is based on the anilinoquinazoline scaffold. This compound displays potency against Src with an IC_{50} value of 10 nM. Dasatinib (BMS-354825), a novel oral and potent multi-targeting inhibitor of Bcr-Abl and Src family kinases (SFK), is a promising cancer therapeutic agent with an IC_{50} of 0.6 nM against Src. Wyeth has developed a dual Bcr-Abl/Src inhibitor, Bosutinib (SKI-606), based on a quinoline scaffold, that is structurally related to the AstraZeneca quinazoline template.[15] This compound displays an IC_{50} of 1.2 nM against Src.

Ligand docking is a method in which the conformational selection of compounds has a high impact on the feasibility of the proposed binding poses. Virtual screening has been established as a valuable in silico technique alongside traditional high-throughput

* Corresponding author. Tel.: +82 2 450 3421; fax: +82 2 447 5987.
E-mail address: ymkim@konkuk.ac.kr (Y. Kim).

0968-0896/$ - see front matter © 2009 Elsevier Ltd. All rights reserved.
doi:10.1016/j.bmc.2009.02.054

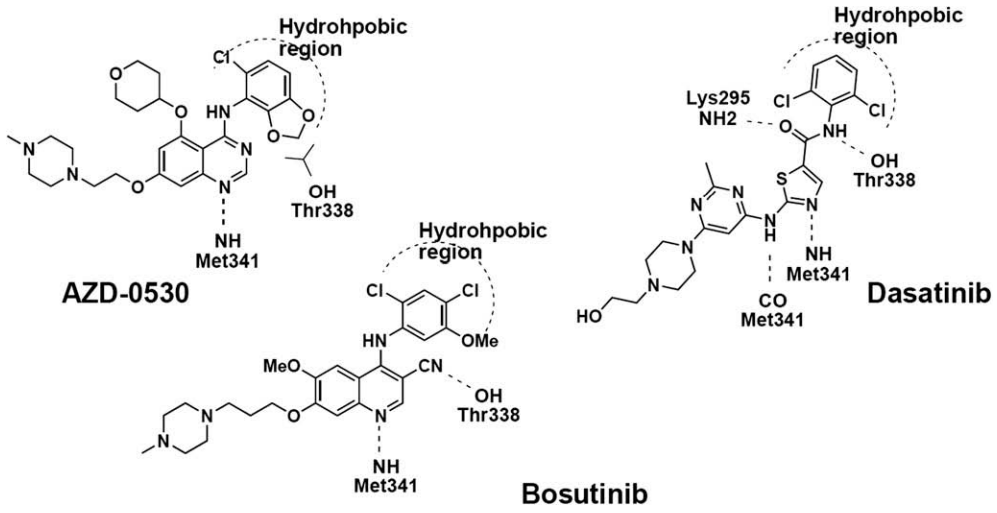

Figure 1. Structures of template inhibitors interacting with the ATP-binding site of Src kinase.

screening for novel active compounds, with increasing success in the pharmaceutical industry.[16,17] Structure-based virtual screening methods are emerging as reliable and complementary approaches to high-throughput screening in the lead discovery process, from hit identification to lead optimization.[18] These processes are performed in two stages: (i) accurate prediction of the pose, and (ii) estimation of tightness of binding (scoring).[19] Once a putative protein–ligand interaction is proposed, a scoring function is used to estimate relative ligand affinity for the target.[20] These screening hits represent a promising source of candidate molecules for evaluation of binding modes by docking and further biological testing.

In this study, we present the computational virtual screening of molecules to identify new potential hits for Src kinase inhibitors, using a docking program. The docking program, LIGANDFIT, was employed to dock hits, and several scoring and consensus scoring functions were applied to evaluate docking results and rank ligand-binding affinities. One novel potential lead was identified on the basis of docking scores and examination of how key interactions are retained for kinase binding.[21] Our results show that this compound is a potent inhibitor of Src, and induces anti-proliferative effects in Src-expressing PC3 human prostate cancer and A431 human epidermoid carcinoma cell lines.

2. Results

Src is one of the few thoroughly characterized and well-validated targets in anti-cancer therapy. The main objective of the present study is to develop a model for virtual screening of Src kinase inhibitors. To achieve this goal within a reasonable timeframe, we needed a rapid and robust docking tool. Our initial studies were performed with the software, LIGANDFIT, widely regarded as one of the best docking programs. The model was further applied for screening an in-house database to identify new leads for Src kinase inhibitors.

2.1. Binding models of compounds 1–3

Recently, several X-ray structures of Src kinase have been determined as complexes with a number of small-molecule inhibitors, including AP23464 and AP23451, purvalanol, CPG77675 and STI-571 (imatinib).[22–24] The X-ray structure of human Src (entry 2H8H) was selected as the starting reference for molecular docking analyses.[13] For a validation of the accuracy of the docking program LIGANDFIT and approach used in this study, the RMS deviation between the crystal structure (PDB 2H8H) and the most reasonable binding modes of AZD-0530 docked with LIGANDFIT was calculated. The results of control docking showed that LIGANDFIT determined the optimal orientation of the docked inhibitor, AZD-0530 to be close to that of the original orientation found in the crystal (Fig. 2). The rms deviation between the experimental docked conformation and the calculated docked conformation for AZD-0530 in Src was 0.34 Å.

Three inhibitors (1–3), Dasatinib (BMS354825; Bristol Meyers Squibb Oncology, Princeton, NY), AZD-0530 (AstraZeneca, Macclesfield, United Kingdom) and Bosutinib (SKI-606; Wyeth Research, Pearl River, NY), were docked onto the optimized structure of Src, and the resulting complexes further minimized to overcome protein rigidity. We evaluated various scoring functions (LigScore1, LigScore2, PLP1, PLP2, and PMF) in an attempt to accurately predict the binding affinities between ligand molecules and their protein receptors. LigScore2 was more successful in retrieving an accurate pose as the top scorer in the LIGANDFIT docking ensemble than were the other functions, and LigScore2 was consequently employed to obtain various scores.

Figure 1 depicts the chemical structures of the three known inhibitors, and interactions between inhibitors and the ATP-binding site of the Src kinase catalytic domain. Inhibitor molecules occupy the ATP-binding site. The quinazoline, quinoline, and pyridine ring templates span the region occupied by the ribose in ATP. The

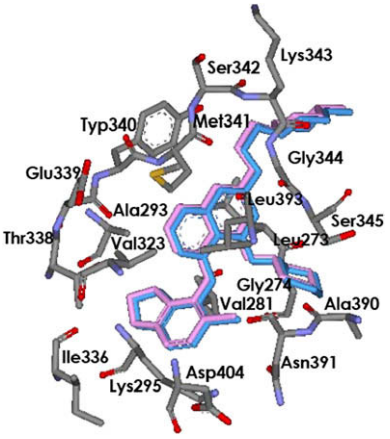

Figure 2. Crystal structure (pink) of AZD-0530 bound to Src compared to the predicted binding mode (blue).

highly conserved hydrogen bond is created by N1 of the ring templates, which binds to the backbone amide of Met341. The cyano group of Bosutinib is hydrogen-bonded to the side-chain OH group of Thr338. Simulations disclose that a network of hydrogen bonds with Met341 and Thr338 restricts the inhibitors within the hinge region of Src, with their molecular scaffolds accommodated within the adenine pocket. Moreover, hydrophobic interactions were identified between anilino moieties and the hydrophobic region formed by Met314, Val323, Ile336, Leu393, Ala403, and Phe405. In Dasatinib, an additional hydrogen bond was identified between the amide carbonyl group and side-chain NH_2 of Lys295. 2-Chloro-6-methylbenzamide occupies a deep hydrophobic pocket.[12] These structural models were useful in providing concrete starting points for further ligand design.

2.2. Identification of hits by virtual screening

Above all the compounds for virtual screening were filtered by applying molecular property filters to eliminate compounds with undesired molecular properties. Src kinase active compounds (candidates and compounds in research states) that have MW 400–500, H-bond donors $\leqslant$2, H-bond acceptors 7–10, 2D polar surface area 65–100, and AlogP 4–5. At first, all compounds were prefiltered according to the criteria. And then to search for similar structures with active compounds we pursued 2D-searching, which is based on chemical similarities. These filters helped in selecting 2300 molecules from a total of 1,561,000 molecules. The concept of molecular physical property filters and similarity are very attractive because of reduced cost, time, reagent, and compound consumption.

Table 1
Docking scores of the reference compound and the final 12 hits obtained from the docking study

Compounds	LigScore2	Src tyrosine kinase (10 μM) positivity
AZD-0530	6.50	
1	6.29	+
2	6.15	+
3	6.01	+
4	6.00	+
5	5.77	–
6	5.78	–
7	5.72	–
8	5.64	–
9	5.82	–
10	5.31	–
11	5.44	–
12	5.86	–

The docking model developed to date provides an accurate idea of the necessary and sufficient molecular attributes required in a new lead. Our objective was to screen a large subset of the corporate collection of compounds. We performed flexible lignad docking with LIGANDFIT on a relatively large library containing 2300 drug-like molecules extracted from optimized commercial and in-house databases. Molecular docking rate was about 65%. Among these, we only considered hit compounds having H-bond with Met341 (major interactions of the Src binding site) and we selected the top-scoring compounds by LigScore2.

Docking calculations of the selected compounds with LIGANDFIT led to the identification of four potent inhibitors with activities in the nanomolar range, producing 12 hits with high LigScore2 (Table 1). Following the above procedure, a dozen compounds were finally selected from chemical archives for actual testing in a Src phosphorylation inhibition assay at a single 10 μM concentration. This prescreen assay aims to eliminate a large proportion of the inactive agents, and preserve 'active' agents. Four of the selected compounds inhibited Src activity at a concentration of 10 μM. Among the four active compounds (shown in Fig. 3), the most potent compound was selected for further investigation. The hit selection process is based not only on potency and novelty, but also on all other parameters that subsequently influence the successful outcome of the lead optimization phase. The hit was further investigated in terms of docking scores, consensus scores, binding conformation, and the degree of fit into the Src kinase-binding site. In particular, how interactions are retained with important amino acid residues (Met341) in the enzyme binding site was considered.

Compound **4,** a quinazolinone derivative synthesized at Hanmi Pharm Co. Ltd, displayed a good docking score (Ligscore2 = 6.00) and most active potency (IC_{50} = 300 nM), supporting its activity as a strong inhibitor of Src kinase. Thus, the virtual screening approach yielded a novel and potent hit class of Src kinase inhibitors from a limited selection of compounds.

2.3. Design and synthesis of analogs

Compound **4**, (*S*)-*N*-(4-(3-chloro-4-fluorophenylamino)-7-(2-methoxyethoxy)qui-nazolin-6-yl)pyrrolidine-2-carboxamide, selected from virtual screening analyses, was employed as a hit for designing

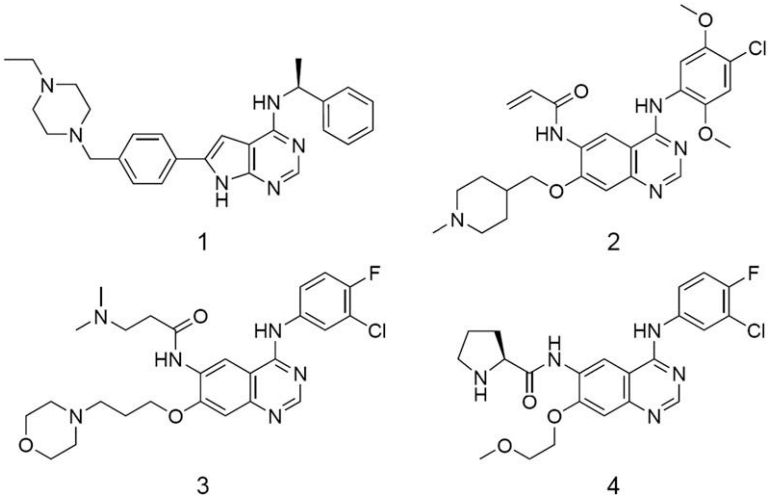

Figure 3. Structures of the final four hits selected from virtual screening and enzyme-based binding affinity assays.

new Src inhibitors. This is a novel anilinoquinazoline compound substituted at the C-6 position of the quinazoline ring. From the structural model, it is hypothesized that the quinazoline ring interacts with the adenine binding site of kinase, whereas the aniline ring is buried in an adjacent hydrophobic pocket. A highly conserved hydrogen bond is created by N1 of quinazoline, which binds to the backbone amide of Met341. Docking of quinazoline-based compounds to the Src model suggests that pyrrolidine rings linked to the C-6 position of quinazoline fit the hydrophobic pocket. Pyrrolidine-NH has one additional interaction with the side-chain carboxyl group of Asp348.

We were able to improve the selectivity of our lead compound by taking advantage of sequence differences among structurally related kinases within the extended hydrophobic pocket. Modification of substituents on the aniline phenyl ring led to dramatic changes in the inhibitory activity against Src kinase.[25,26] To gain an insight into the structural basis of the inhibitory activities of our aniline series, we performed molecular modeling and docking studies using the available 3D structure of Src kinase.[13]

We uses sets of pre-defined molecular building blocks that are connected by a virtual synthesis scheme.[19] On the basis of published experimental data, we have built a small focused library (Table 2). The preferred conformation was analyzed by varying the aniline or bicyclic aniline substituents at C-4 of quinazoline.

Manipulation of the aniline substitution patterns has allowed the discovery of a potent and selective Src inhibitor. The structure-guided approaches to fragment optimization rapidly generate compounds with increased potency, from initial low activity for fragment hits to nanomolar activities that are usually associated with high-quality lead molecules. Virtual compounds were generated from compound **4** with 33 aromatic ring groups at C-4. Next, docking studies were performed on the compounds. In view of the structural similarity and binding affinity to Src, compound **43** was

Table 2
Analog design for hit optimization

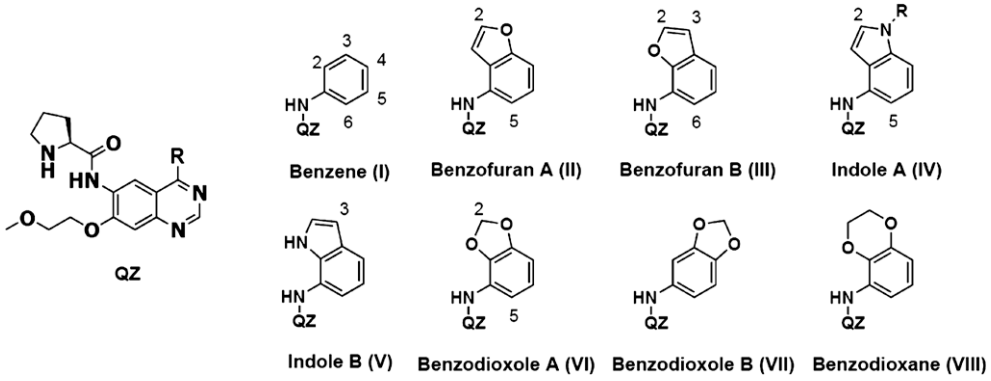

No.		R					LigScore2
		2	3	4	5	6	
13	I			Cl		Cl	5.81
14	I					Cl	5.43
15	I			Cl			5.97
16	I				Cl	Cl	6.08
17	I		Cl			Cl	6.01
18	I	Cl				Cl	5.80
19	I		Cl		Cl		5.50
20	I			Cl	Cl		6.09
21	I			Cl		F	5.77
22	I			Cl		Br	5.86
23	I			Cl		I	5.81
24	I			I		Cl	5.66
25	I			Br		Cl	5.90
26	I		OMe	OMe	OMe		5.22
27	I		OMe	Cl		Br	5.83
28	I		OMe			Cl	6.09
29	I		OMe				5.69
30	I					OMe	5.48
31	I			OMe			5.49
32	I		OEt			Cl	5.66
33	II						5.93
34	II				Cl		5.71
35	III						6.04
36	III				Cl		5.95
37	III		Cl				6.05
38	IV	H					5.94
39	IV	Me					5.99
40	V						6.01
41	V		Cl				5.94
42	VI						5.75
43	VI				Cl		6.14
44	VII						5.81
45	VIII						5.53

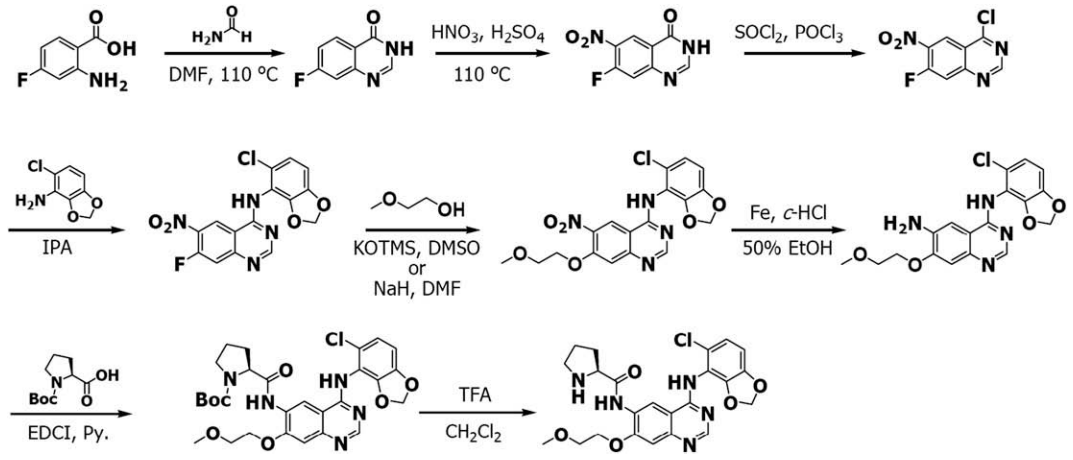

Scheme 1. Synthesis of (*S*)-pyrrolidine-2-carboxylic acid [4-(5-chloro-benzo[1,3]dioxol-4-ylamino)-7-(2-methoxy-ethoxy)-quinazolin-6-yl]-amide.

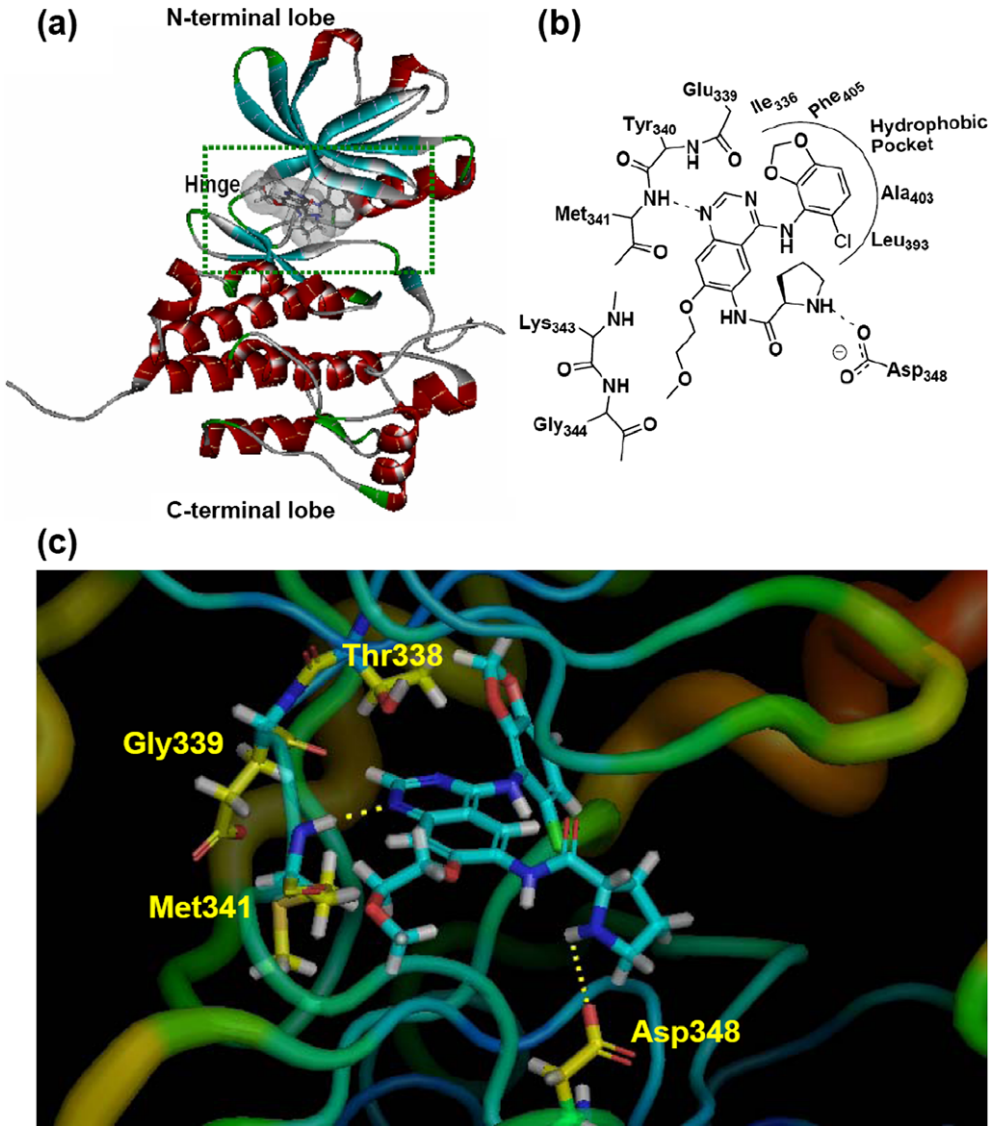

Figure 4. (a) Ribbon diagram illustrating the crystal structure of human Src,[13] with compound **43** bound to the active site. (b) Two-dimensional representation of the interacting mode of compound **43** with Src. The quinazoline ring occupies the adenine binding site. The H-bond interaction between quinazoline N1 and backbone NH of Met341 is presented as a dotted line. (c) Graphical representation of the binding mode of compound **43** to the ATP-binding site of Src. For clarity, only a few residues are displayed, and hydrogen bond interactions are represented by yellow dashed lines.

established as a new potential lead for Src-selective inhibition on the basis of LigScore2 docking scores. The benzodioxole heterocycle is buried in the hydrophobic pocket containing Met314, Val323, Ile336, Leu393, Ala403, and Phe405. This potential lead is expected to possess strong selectivity for Src. The compound was synthesized through the route outlined in Scheme 1, and details of the synthetic procedures and structural characterizations are described in Section 4.

2.4. Binding models

The lead compound **43** was docked onto the Src kinase-binding site, and regions of favorable protein–ligand interactions were visually analyzed. The results indicate that the compound docks well and interacts with important residues of the Src kinase-binding site (Fig. 4). Whereas hydrogen bonding is essential for this mode of inhibition, the number of hydrogen bonds between the protein and ligand is not correlated with potency.[13]

We additionally used a binding model and conformation analysis to determine the importance of interactions between inhibitors and enzymes. The docking structure of the active Src kinase domain in complex with compound **43** shows that the quinazoline ring occupies the adenine binding site, similar to results derived from crystallographic analyses (Fig. 4a). The Src kinase domain adopts an elongated bilobed structure typical of all kinases.

Binding Mode of quinazolines in Src kinase has been extensively studied.[13,25] A highly conserved hydrogen bond is created by N1 of the quinazoline, which binds to the backbone amide of Met341. In addition, the compound binds in the predicted orientation and satisfies the expected hydrophobic and aromatic interactions (Fig. 4b and c). As predicted based on information about quinazoline inhibitors, a bulky C-4 aniline is necessary to target Src kinase.7 The aniline NH is not involved in direct hydrogen-bonding interactions with the protein. The chlorobenzodioxole moiety fits tightly into the hydrophobic pocket formed by Met314, Val323, Ile336, Leu393, Ala403, and Phe405, as shown in Figure 3b. In this study, we further investigate a novel series of anilinoquinazolines substituted at the C-6 position of the quinazoline ring. The C-6 position allows access to the ATP ribose binding site, and may thus provide the enzyme with additional binding affinity. The pyrrolidine ring of the C-6 quinazoline appears to fit tightly in a hydrophobic pocket. Hydrophobic interactions with the protein are predominant, with one additional hydrogen bond between pyrrolidine NH and the side-chain carboxyl group of Asp348. Buried hydrophobic surface areas between the protein and ligand in the pyrrolidine ring region may account for the increase in binding affinity. Docking studies of potential inhibitors onto our 3D model of Src revealed that heterocycles linked to the C-6 position of the quinazoline fit the shape of the ribose pocket. Moreover, the C-7 side chain of the molecule is directed towards the solvent-exposed region. These findings prove that the solubilizing groups of flexible side chains enhance in vitro potency, and optimize the physicochemical properties of this compound series.[27,28,6]

2.5. Biological activities

To further establish compound **43** enzyme inhibitory properties, the compound was evaluated for selectivity against in-house kinases, as shown in Table 3. The inhibitory activity of compound **43** on Src was more potent than those of EGFR (IC50 = 7.1 μM) and VEGFR-2 (no inhibition at 10 μM). The compound was highly selective for Src, compared to EGFR (IC50 ratio > 80-fold) and VEGFR-2 (IC50 ratio > 110-fold). These findings provide valuable information for the design of selective and powerful ATP-competitive inhibitors of Src kinases.

Table 3
Selectivity profile of compound **43**

Compound	Enzyme (μM)		
	Src	EGFR	VEGFR-2
43	0.089	7.13	No inhibition
Dasatinib	0.014	2.87	2.36
AZD-0530	0.003	2.60	21.00

Src signaling is a key pathway during normal and dysregulated bone functioning, and bone metastases are responsible for substantial morbidity in advanced prostate and melanoma cancers. Thus, Src inhibition represents a potentially useful therapeutic strategy for patients in various stages of prostate cancer. PC3 cells are derived from a human prostate cancer bone metastasis. Oncogenic signaling of EGFR in A431 cells may contribute to the elevated activation of Src family kinases. PC3 and A431 cells were treated with various concentrations of compound **43** to assess its anti-proliferative effects. We observed dose-dependent inhibitory effects on the growth of PC3 and A431 cells (Fig. 5a). Moreover, inhibition of EGF-stimulated total cellular tyrosine phosphorylation in A431 cells was evident at a submicromolar level of compound **43** (0.78 μM). However, the compound exerted no inhibitory effects on SK-Br3, a cell line in which the HER2 protein is highly expressed, or MCF-7, a human breast adenocarcinoma cell line (<10 μM, data not shown). As extracellular signal-regulated kinase (ERK), which acts downstream of Src kinase, is involved in cell proliferation, we investigated whether compound **43** affects the

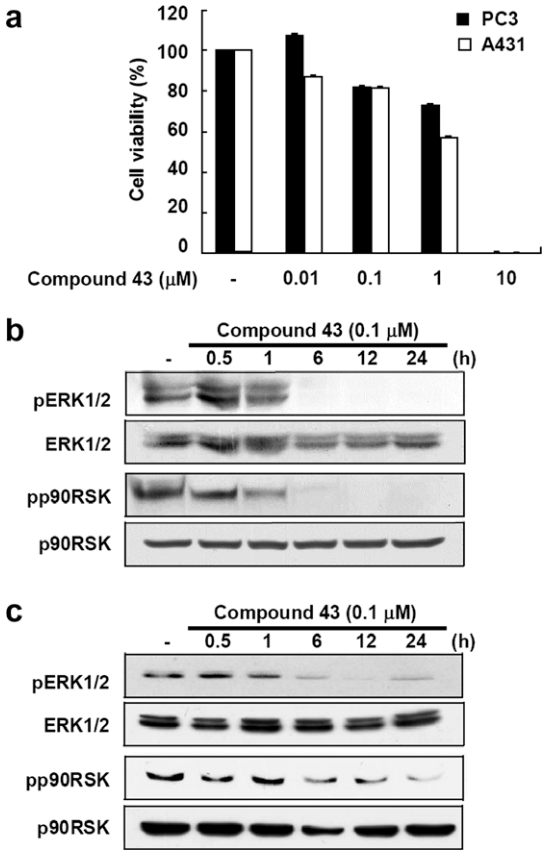

Figure 5. (a) Viability of PC3 and A431 cells treated with compound **43**. Cells were treated with the specified concentrations of compound **43** for 72 h, and viability determined with the SRB assay. Effects of compound **43** on ERK-p90RSK phosphorylation in (b) PC3 and (c) A431 cells. Cells were treated with 0.1 μM compound **43** for the indicated times, lysed, and the levels of phosphorylated and total ERK and p90RSK proteins determined by Western blot analysis using specific antibodies.

Table 4
Pharmacokinetic properties of compound **43** in Sprague–Dawley rats

	AUC (μg h/mL)	C_{max} (μM)	T_{max} (h)	$t_{1/2}$ (h)	F (%)
IV(5 mg/kg)	2.40	2.01	0.08	6.1	–
PO (10 mg/kg)	1.24	0.12	4.0	5.4	20.4

phosphorylation of ERK and p90RSK, a downstream signal of ERK, in PC3 and A431 cells. Notably, compound **43** (0.1 μM) attenuated ERK and p90RSK phosphorylation in a time-dependent manner. After 6 h, complete inhibition of ERK and p90RSK phosphorylation was observed in PC3 and A431 cells (Fig. 5b and c). The results collectively indicate that compound **43** strongly inhibits Src kinase activity, leading to suppression of Src downstream signals, ERK and p90RSK, and tumor cell proliferation.

2.6. Rat pharmacokinetic studies

Based on the initial screening data, a pharmacokinetic (PK) study on compound **43** was performed in rats (Table 4). Upon administration of single doses of 10 mg/kg (iv and po), the compound displayed peak plasma exposure of 0.4 mM (C_{max}) with a T_{max} of 1 h. Oral bioavailability of **43** in rats was determined as 20%. Although this novel compound is not yet considered to be a potential clinical candidate, the molecular scaffold combined with specific biological properties allows it to be classified as a promising hit for the further development of effective tyrosine kinase inhibitors.

3. Conclusions

A structure-based virtual screening approach has facilitated the identification of compounds that effectively inhibit Src kinase activity. A computational docking study was structured to optimize the efficiency of each step in terms of time and costs. A virtual screening application is presented, leading to the successful identification of novel nanomolar Src kinase inhibitors. The approach employed structure-based screening of an in-house kinase database. The software package, LIGANDFIT, was used for the identification and visualization of protein–ligand interaction sites and database searching.

LIGANDFIT docking analysis of BMS354825, AZD-0530, and SKI-606 confirmed that these ligands have a reasonable fit into the binding site of Src kinase. We identified a C-6 substituted quinazoline compound as a novel strong inhibitor of protein Src kinase by virtual screening. We selected the hit compound **4** (300 nM) as the template for the design of new Src kinase inhibitors for further synthetic work.

Substituents at position 4 of the heterocyclic core were synthesized for optimization of anti-proliferative activity, and evaluated as Src kinase inhibitors. We discovered highly potent and selective inhibitors of Src through docking studies, synthesis, and enzyme-based assays. Specifically, compound **43** inhibited Src activity with enzyme-based assay. The docking structure of a low nanomolar IC_{50} values (IC_{50} = 89 nM) in an complex of compound **43** and Src disclosed a highly conserved hydrogen bond created by N1 of quinazoline, which interacts with the backbone amide of Met341. In addition, the pyrrolidine ring of the C-6 quinazoline appears to fit tightly within a hydrophobic pocket. One additional hydrogen bond between compound **43** and the side-chain carboxyl oxygen of Asp348 of the protein is proposed. The buried hydrophobic surface areas of both protein and ligand in the region of the pyrrolidine ring may account for the increased binding affinity.

Src signaling is a major pathway involved in tumor proliferation and progression. Activation of Src signaling is responsible for considerable morbidity in advanced prostate cancer. Oncogenic signaling of EGFR in A431 cells may contribute to the elevated activation of Src family kinases. ERK and p90RSK, downstream signals of Src, contribute to cell proliferation, motility, and invasion of tumor cells. In our experiments, compound **43** strongly suppressed cell proliferation and inhibited phosphorylation of ERK and p90RSK in a time-dependent manner in PC3 and A431 cells. These results indicate that inhibition of Src kinase activity by compound **43** leads to the downregulation of ERK and p90RSK phosphorylation, and eventual suppression of PC3 and A431 cell proliferation.

Thus, we conclude that large database docking, in conjunction with appropriate scoring and filtering processes, is useful in medicinal chemistry. This approach has reached an advanced stage, where it may effectively contribute to the lead discovery process. Further optimization and SAR studies to improve cellular and in vivo potency are ongoing.

4. Experimental

4.1. Generation of ligand and enzyme structures

Virtual screening by docking requires an accurate three-dimensional (3D) target structure. The crystal structure of Src kinase domain bound to its inhibitor, AZD-0530, *N*-(5-chloro-1,3-benzodioxol-4-yl)-7-[2-(4-methylpipe-razin-1-yl)ethoxy]-5-(tetrahydro-2*H*-pyran-4-yloxy)qui-nazolin-4-amine, was obtained from the Protein Data Bank (PDB entry 2H8H).[13] Initially, hydrogen atoms were added to the protein, assuming that all the residues were in the neutral form. All water molecules in the active site were included. The protein was subjected to minimization using the steepest descent (gradient <0.1), and conjugate gradient algorithms (gradient <0.01) with the CHARMM force field in INSIGHTII.[29] The Src active site was defined using the inhibitor, AZD-0530 *N*-(5-chloro-1,3-benzodioxol-4-yl)-7-[2-(4-methylpiperazin-1-yl)ethoxy]-5-(tetrahydro-2*H*-pyran-4-yloxy)quinazo-lin-4-amine, and included all residues within a 10 Å radius from the center of the ligand. The protein active site conformations with the ligands were retrieved for further analysis.

4.2. Compound collection

We analyzed the physicochemical profiles of 1,561,000 compounds for virtual screening. Various commercially compounds were compiled. Compound collections have been enriched and enlarged through commercial available databases, namely, AMRI (175,000), Asinex (358,000), Enamine (400,000), InterBioScreen (322,000), Life Chemicals (296,000)[30] and in-house (10,000) synthesis. Although the docking protocol has been developed internally in several case studies, and is able to rank known inhibitors for similar targets at the top of the hit list, in this case, we applied all the post- processing filtering and reranking tasks recommended to increase the hit rate in a docking study.[31] To design compounds with good oral bioavailability amenable for chronic oral administration, we focused on the molecular properties that affect absorption, such as 2D polar surface area (PSA), AlogP, molecular weight (MW), H-bond donor-acceptor (HBDA) properties, and number of rotatable bonds.[32] The physical properties and chemical similarities were calculated with DS Accord for Excel 6 Add-in tools from Accelrys Inc., San Diego, CA, USA.

4.3. LIGANDFIT docking and scoring

Virtual screening is one of the important strategies for hit identification and lead optimization. A schematic diagram representing the virtual screening strategy is shown in Figure 6. LIGANDFIT from Discovery Studio 1.7 version (Accelrys, San Diego, USA) was applied for all runs. Reference protein coordinates for docking were

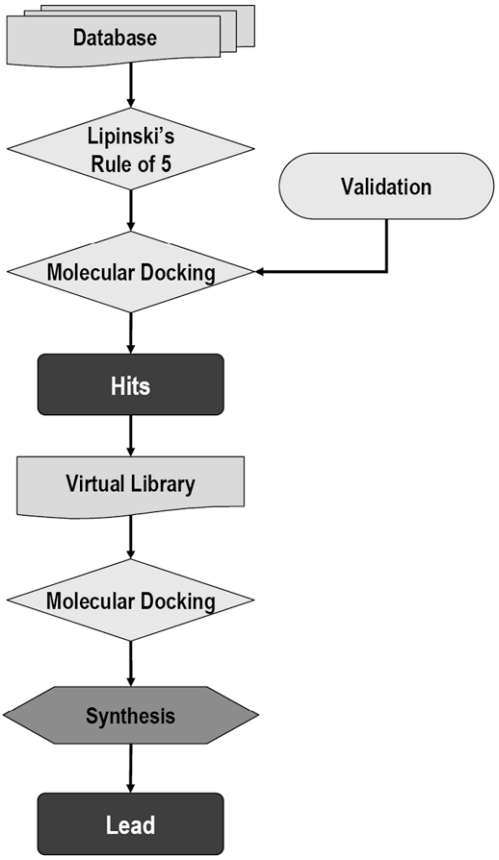

Figure 6. Schematic representation of the virtual screening strategy.

obtained from the X-ray structures of Src kinase complexed with 4-amino-quinazoline. The docking site search was performed in the shape-based mode based on the crystal structure of the compound, 4-amino-quinazoline. All calculations were performed with the CFF 1.01 force field. Conformations were generated with Monte Carlo simulations (10,000 trials), and Flexible fit was selected.

The grid resolution was set to 0.5 Å. The default rigid body minimization parameters were used to dock the four orientations of each conformation into the site, followed by 500-step final minimization of each docked ligand. Scoring was performed for each of the 10 saved ligand conformations using a set of functions, as implemented in Discovery Studio 1.7, including LigScore1, LigScore2, PLP1, PLP2, JAIN, PMF, and LUDI.[33–35]

4.4. Virtual library construction and docking study

Our initial hits obtained with virtual screening belonged to the anilinoquinazoline family (Fig. 3, compound **4**). Virtual compounds for hit-to-lead were generated from compound **4** with **33** aromatic ring groups at C-4 to ensure activity and selectivity for Src kinase. Aromatic rings were selected with various substituent patterns (Table 2).[25] The molecular structure was minimized with the CHARMM force field program (Accelrys, Inc. Sandiego, USA). All docking simulations for the methods are presented above. LigScore2 was applied for the selection of scoring functions in further docking studies of Src kinase inhibitors into the protein active site.

4.5. In vitro Src kinase inhibition test

An enzyme selectivity screen was performed with the Src kinase assay kit (Promega, Madison, USA). Reactions were performed in 96-well polystyrene round-bottomed plates. Briefly, test compounds were added to a plate in the presence of ATP and specific substrates in kinase solution, and incubated for 1 h at room temperature before the addition of protease solution. After the application of stabilizer solution, fluorescence polarization values were measured at 485/530 nm using a fluorescence reader. All compounds were dissolved in DMSO and diluted in buffer, yielding a final DMSO concentration of 1% in the assay.

4.6. In vitro growth inhibition assay

PC3 cells were obtained from the Korean Cell Line Bank (Seoul, Republic of Korea). A431 and SK-BR3 cells were obtained from the American Type Culture Collection (Rockville, MD). PC3 and SK-BR3 cells were maintained in RPMI 1640 supplemented with 10% fetal bovine serum (FBS, Gibco BRL), 100 units/mL penicillin, and 100 μg/mL streptomycin sulfate. A431 and MCF-7 cells were maintained in DMEM containing 10% FBS. For assessment of cell-based potency, cells were plated on a 96-well plate (Corning costar) at densities ranging from 10,000 to 15,000 cells/well. The microtiter plates were incubated at 37 °C under 5% CO_2. After 24 h, the drug was added at the indicated concentrations. After 72 h, reactions were terminated by the addition of cold 10% trichloro-acetic acid. Plates were washed with flowing deionized water and air-dried. Sulforhodamine B solution (0.4% w/v in 1% acetic acid) was added to each well, and unbound dye washed out. The bound stain was subsequently solubilized with 10 mM Trizma base, and the absorbance read on an automated plate reader. Growth inhibition of 50% (GI50) was calculated, based on the following equation: $[(Ti - Tz)/(C - Tz)] \times 100 = 50$ (Ti: test growth, Tz: time zero, C: control growth).

4.7. Western blot analysis

PC3 and A431 cells were cultured in 6 cm dishes for 48 h, followed by treatment with compound **43** (0.1 μM) for different time-periods. Cell lysates were scraped and treated with lysis buffer (10 mM Tris, pH 7.5; 150 mM NaCl; 5 mM EDTA; 1% Triton X-100; 1 mM DTT; 0.1 mM PMSF; 10% glycerol; and a protease inhibitor cocktail tablet) on ice, followed by centrifugation at 14,000 rpm for 10 min. Protein concentrations in the supernatant were determined using a dye-binding protein assay kit (Bio-Rad Laboratories Hercules, CA), as described in the manufacturer's manual. Lysate proteins were subjected to 10% sodium dodecyl sulfate (SDS)–polyacrylamide gel electrophoresis (PAGE), and electrophoretically transferred to PVDF membrane (Millipore Corporation, Bedford, MA, USA). After blotting, the membrane was blocked in 5% fat-free dry milk for 1 h, and incubated with the specific primary antibody for 2 h at room temperature. Protein bands were detected using the enhanced chemiluminescence (ECL) detection kit (Amersham, Piscataway, NJ) after hybridization with the HRP-conjugated secondary antibody.

4.8. Rat pharmacokinetics

Adult male Sprague-Dawley rats were obtained from Orient Co. (Gyeonggi-do, Korea), and had free access to pellet chow (Picolab rodent diet 5053) and tap water. Throughout the experiments, animals were housed in laminar flow cages (three per cage) maintained at 22 ± 2 °C, 50 ± 20% relative humidity, under a 12 h light/12 h dark cycle. Animals were kept in these facilities for at least one week prior to the experiment. For the oral study, rats were starved overnight prior to dosing and fed approximately 2 h after dosing. Rats were not subjected to fasting for the intravenous study. The vehicle for intravenous (IV) and oral dosing

was 23% ERi vehicle (PEG 200 with 0.02 5% cHCl/Tween 80 (20:3, v/v). Blood samples were collected at various times after IV and oral dosing. Approximately 0.3 mL of blood was collected from the tail vein in tubes containing heparin, and plasma obtained by centrifugation. Plasma samples were stored at −80 °C until use. Samples were analyzed for compound **43** by LCMS. The time elapsed to peak (T_{max}) and maximum concentration (C_{max}) were obtained directly from the observed value. The half-life ($t_{1/2}$) was calculated using the elimination rate constant (Ke), which, in turn, was estimated by regression analysis from the slope of the line. The half-life value was obtained from 0.693/Ke. The area under the curve was computed by the linear trapezoidal rule from 0 to 5 h (AUC5). The value of AUC_{∞} was calculated as AUC5 + [plasma concentration at 5 h after dosing/elimination rate constant].

4.9. Chemistry

4.9.1. 7-Fluoro-3*H*-quinazolin-4-one

A catalytic amount (1 ml) of *N*,*N*-dimethylamide was added to a solution of 2-amino-4-fluorobenzoic acid (50 g, 322 mmol) and formamide (77 mL, 1934 mmol), and the resulting solution stirred. The solution was heated to 180 °C and stirred for 14 h. The solution was cooled to room temperature, and 300 mL of distilled water added. The resulting mixture was stirred for about 30 min, and filtered to obtain 7-fluoro-3*H*-quinazolin-4-one (41.3 g, yield: 78%). ^{1}H NMR (DMSO-d_6) δ: 7.47–7.35 (m, 2H), 8.20–8.13 (m, 2H), 11.85 (br s, 1H).

4.9.2. 7-Fluoro-6-nitro-3*H*-quinazolin-4-one

7-Fluoro-3*H*-quinazolin-4-one (25 g, 152 mmol) was added to a mixture of concentrated sulfuric acid (50 mL) and fuming nitric acid (51 mL) at 0 °C. The resulting solution was stirred at room temperature for 1 h, heated to 110 °C and stirred for 2 h. The solution was cooled to room temperature, and 300 mL of ice water added. The resulting mixture was stirred for about 30 min, and filtered to obtain 7-fluoro-6-nitro-3*H*-quinazolin-4-one (25 g, yield: 79%). ^{1}H NMR ($CDCl_3$) δ: 7.79 (d, 1H), 8.32 (s, 1H), 8.72 (d, 1H), 12.83 (br s, 1H).

4.9.3. 4-Chloro-7-fluoro-6-nitro-quinazoline

7-Fluoro-6-nitro-3*H*-quinazolin-4-one (20 g, 96 mmol), thionyl chloride (170 mL), phosphorous oxychloride (30 mL) and *N*,*N*-dimethylformamide (1 mL) were added to a reaction bottle and stirred. The resulting solution was heated to 100 °C until the solid was dissolved, followed by stirring for 2 h. The reaction was cooled to room temperature, and the solvent removed under reduced pressure. The resulting residue was re-distilled after adding 300 mL of toluene, and the procedure repeated three times to obtain 4-chloro-7-fluoro-6-nitro-quinazoline (21 g, yield: 99%). ^{1}H NMR ($CDCl_3$) δ: 7.73 (d, 1H), 8.30 (s, 1H), 8.72 (d, 1H).

4.9.4. (5-Chloro-benzo[1,3]dioxol-4-yl)-(7-fluoro-6-nitro-quinazolin-4-yl)-amine

4-Chloro-7-fluoro-6-nitro-quinazoline (1.67 g, 7.42 mmol) and 5-chloro-benzo-[1,3]dioxloe-4-ylamine[23] (1.27 g, 7.42 mmol) were added to 2-propanol (15 mL). The reaction mixture was heated to reflux for 2 h after the addition of 6 N HCl (1.5 mL), cooled to room temperature, and made basic with saturated $NaHCO_3$ (aq). Next, the mixture was extracted with ethyl acetate (20 mL × 3), and washed with brine. The organic layer was dried over $MgSO_4$. The filtrate was concentrated in vacuo to yield 5-chloro-benzo[1,3]dioxol-4-yl)-(7-fluoro-6-nitro-quinazolin-4-yl)-amine (2.4 g, 89%). ^{1}H NMR (DMSO-d_6) δ: 10.60 (s, 1H), 10.11(d, J = 8.1 Hz, 1H), 8.61 (s, 1H), 8.32 (s, 1H), 7.12 (d, J = 6 Hz, 1H), 7.00 (d, J = 6 Hz, 1H), 6.10 (s, 2H).

4.9.5. (5-Chloro-benzo[1,3]dioxol-4-yl)-[7-(2-methoxy-ethoxy)-6-nitro-quinazolin-4-yl]-amine

Potassium trimethylsilanoate (3.40 g, 26.5 mmol) was added to a mixture of (5-chloro-benzo[1,3]dioxol-4-yl)-(7-fluoro-6-nitro-quinazolin-4-yl)-amine (2.4 g, 6.62 mmol) and 2-methoxy-ethanol (1.57 mL, 19.9 mmol) in dimethylsulfoxide (50 mL). After stirring for 4 h, the reaction was quenched with water, and the mixture extracted with ethyl acetate (30 mL × 3). The organic layer was washed with water (30 mL × 4) and brine (30 mL), and dried over $MgSO_4$. The filtrate was concentrated in vacuo. The residue was purified by flash chromatography to yield 5-chloro-benzo[1,3]dioxol-4-yl)-[7-(2-methoxy-ethoxy)-6-nitro-quinazolin-4-yl]-amine (1,.44 g, 52%). ^{1}H NMR (DMSO-d_6) δ: 10.18 (s, 1H), 9.30 (s, 1H), 8.52 (s, 1H), 7.52 (s, 1H), 7.08 (d, J = 7.5 Hz, 1H), 7.00 (d, J = 7.5 Hz, 1H), 6.25 (s, 2H), 4.43 (m, 2H), 3.75 (m, 2H), 3.31 (s, 3H).

4.9.6. N4-(5-Chloro-benzo[1,3]dioxol-4-yl)-7-(2-methoxy-ethoxy)-quinazoline-4,6-diamine

Concentrated HCl (0.115 mL) was added to a mixture of iron (961 mg, 17.2 mmol) in 50% ethanol (aq) (20 mL). The mixture was heated to reflux for 1 h. 5-Chloro-benzo[1,3]dioxol-4-yl)-[7-(2-methoxy-ethoxy)-6-nitro-quinazolin-4-yl]-amine (1.44 g, 3.43 mmol) was added to the reaction mixture and stirred continuously for 1 h at the same temperature. The reaction mixture was hot-filtered through Celite, and the filtrate cooled to room temperature. The mixture was made basic with saturated $NaHCO_3$ (aq), and extracted with ethyl acetate (20 mL × 3). The organic layer was washed with water and brine, and dried over $MgSO_4$. Next, the mixture was concentrated in vacuo to yield N4-(5-chloro-benzo[1,3]dioxol-4-yl)-7-(2-methoxy-ethoxy)-quinazoline-4,6-diamine (1.25 g, 95%). ^{1}H NMR (DMSO-d_6) δ: 9.12 (s, 1H), 8.12 (s, 1H), 7.35 (s, 1H), 7.13 (s, 1H), 7.08 (d, J = 7.5 Hz, 1H), 6.80 (d, J = 7.5 Hz, 1H), 6.05 (s, 2H), 5.23 (s, 2H), 4.43 (m, 2H), 3.75 (m, 2H), 3.31 (s, 3H).

4.9.7. (*S*)-2-[4-(5-Chloro-benzo[1,3]dioxol-4-ylamino)-7-(2-methoxy-ethoxy)-quinazolin-6-ylcarbamoyl]-pyrrolidine-1-carboxylic acid *tert*-butyl ester

N4-(5-chloro-benzo[1,3]dioxol-4-yl)-7-(2-methoxy-ethoxy)-quinazoline-4,6-diamine (200 mg, 0.342 mmol) was added to the reaction mixture of Boc-L-proline (219 mg, 0.512 mmol) and 1-(3-diethylaminopropyl)-3-ethylcarbodiimide HCl (295 mg, 0.684 mmol) in pyridine (3 mL). The mixture was stirred for 2 h, and the reaction quenched with water. Next, the mixture was extracted with ethyl acetate, and the organic layer was washed with brine, dried over $MgSO_4$, and evaporated in vacuo. The residue was purified by flash chromatography to yield 2-[4-(5-chloro-benzo[1,3]dioxol-4-ylamino)-7-(2-methoxy-ethoxy)-quinazolin-6-ylcarbamoyl]-pyrrolidine-1-carboxylic acid *tert*-butyl ester (150 mg, 75%). ^{1}H NMR ($CDCl_3$) δ: 9.08 (s, 1H), 8.60 (s, 1H), 7.26 (m, 1H), 7.03 (s, 1H), 6.95 (d, J = 7.5 Hz, 1H), 6.65 (d, J = 7.5 Hz, 1H), 6.00 (s, 2H), 4.33 (m, 3H), 3.85 (m, 2H), 3.50 (m, 5H), 2.30–1.80 (m, 4H), 1.70–1.40 (m, 9H).

4.9.8. (*S*)-Pyrrolidine-2-carboxylic acid [4-(5-chloro-benzo[1,3]dioxol-4-ylamino)-7-(2-methoxy-ethoxy)-quinazolin-6-yl]-amide

2-[4-(5-Chloro-benzo[1,3]dioxol-4-ylamino)-7-(2-methoxy-ethoxy)-quinazolin-6-ylcarbamoyl]-pyrrolidine-1-carboxylic acid *tert*-butyl ester (150 mg, 0.256 mmol) was diluted with dichloromethane (3 mL). Trifluoroacetic acid (3 mL) was added drop-wise into the reaction mixture, followed by stirring for 1 h. The solvent was removed through evaporation in vacuo. The residue was diluted with ethyl acetate (10 mL) and made basic with saturated $NaHCO_3$ (aq). Layers were separated, the organic layer washed with brine and dried over $MgSO_4$. The mixture was concentrated in vacuo to yield pyrrolidine-2-carboxylic acid [4-(5-chloro-

benzo[1,3]dioxol-4-ylamino)-7-(2-methoxy-ethoxy)-quinazolin-6-yl]-amide (60 mg, 48%). ^{1}H NMR (CD_3OD) δ: 8.95 (s, 1H), 8.31 (s, 1H), 7.26 (s, 1H), 7.03 (d, J = 7.5 Hz, 1H), 6.85 (d, J = 7.5 Hz, 1H), 6.01 (s, 2H), 4.39 (m, 2H), 4.10 (m, 1H), 3.91 (m, 2H), 3.46 (s, 3H), 3,29 (m, 2H), 2.30 (m, 1H), 2.00–1.87 (m, 3H).

Acknowledgment

This work was supported by a Research Program for New Drug Target Discovery grant (M10601000153-07N0100-15310).

References and notes

1. Hunter, T.; Sefton, B. M. *Proc. Natl. Acad. Sci. U.S.A.* **1980**, *77*, 1311.
2. Schwartzberg, P. L. *Oncogene* **1998**, *17*, 1463.
3. Thomas, S. M.; Brugge, J. S. *Annu. Rev. Cell Dev. Biol.* **1997**, *13*, 513.
4. Boggon, T. J.; Eck, M. J. *Oncogene* **2004**, *23*, 7918.
5. Parsons, S. J.; Parsons, J. T. *Oncogene* **2004**, *23*, 7906.
6. Summy, J. M.; Gallick, G. E. *Cancer Metastasis Rev.* **2003**, *22*, 337.
7. Zhang, Q.; Thomas, S. M.; Xi, S.; Smithgall, T. E.; Siegfried, J. M.; Kamens, J.; Gooding, W. E.; Grandis, J. R. *Cancer Res.* **2004**, *64*, 6166.
8. Golas, J. M.; Lucas, J.; Etienne, C.; Golas, J.; Discafani, C.; Sridhara, L.; Boghaert, E.; Arndt, K.; Ye, F.; Boschelli, D. H.; Li, F.; Titsch, C. *Cancer Res.* **2005**, *65*, 5358.
9. Brunton, V. G.; Avizienyte, E.; Fincham, V. J.; Serrels, B.; Metcalf, C. A., III; Sawyer, T. K.; Frame, M. C. *Cancer Res.* **2005**, *65*, 1335.
10. Lesslie, D. P.; Summy, J. M.; Parikh, N. U.; Trevino, J. G.; Sawyer, T. K.; Metcalf, C. A.; Shakespeare, W. C.; Hicklin, D. J.; Ellis, L. M.; Gallick, G. E. *Br. J. Cancer* **2006**, *94*, 1710.
11. Sawyer, T. K.; Bohacek, R. S.; Metcalf, C. A., III; Shakespeare, W. C.; Wang, Y.; Sundaramoorthi, R.; Keenan, T.; Narula, S.; Weigele, M.; Dalgarno, D. C. *Biotechniques* **2003**, *2–10*, 12.
12. Lombardo, L. J.; Lee, F. Y.; Chen, P.; Norris, D.; Barrish, J. C.; Behnia, K.; Castaneda, S.; Cornelius, L. A.; Das, J.; Doweyko, A. M.; Fairchild, C.; Hunt, J. T.; Inigo, I.; Johnston, K.; Kamath, A.; Kan, D.; Klei, H.; Marathe, P.; Pang, S.; Peterson, R.; Pitt, S.; Schieven, G. L.; Schmidt, R. J.; Tokarski, J.; Wen, M. L.; Wityak, J.; Borzilleri, R. M. *J. Med. Chem.* **2004**, *47*, 6658.
13. Hennequin, L. F.; Allen, J.; Breed, J.; Curwen, J.; Fennell, M.; Green, T. P.; Lambert-van der Brempt, C.; Morgentin, R.; Norman, R. A.; Olivier, A.; Otterbein, L.; Ple, P. A.; Warin, N.; Costello, G. *J. Med. Chem.* **2006**, *49*, 6465.
14. Boschelli, D. H.; Ye, F.; Wang, Y. D.; Dutia, M.; Johnson, S. L.; Wu, B.; Miller, K.; Powell, D. W.; Yaczko, D.; Young, M.; Tischler, M.; Arndt, K.; Discafani, C.; Etienne, C.; Gibbons, J.; Grod, J.; Lucas, J.; Weber, J. M.; Boschelli, F. *J. Med. Chem.* **2001**, *44*, 3965.
15. Paul William Manley, P. W.; Cowan-Jacob, S. W.; Mestan, J. *Biochim. Biophys. Acta* **2005**, *1754*, 3.
16. Shoichet, B. K. *Nature* **2004**, *432*, 862.
17. Oprea, T. I.; Matter, H. *Curr. Opin. Chem. Biol.* **2004**, *8*, 349.
18. Bajorath, J. *Nat. Rev. Drug Disc.* **2002**, *1*, 882.
19. Schneider, G.; Bohm, H. J. *DDT* **2002**, *7*, 64.
20. Ajay, A. J.; Murcko, M. A. *J. Med. Chem.* **1995**, *38*, 4953.
21. Yu, H.; Wang, Z.; Zhang, L.; Zhang, J.; Huang, Q. *Chem. Biol. Drug Des.* **2007**, *69*, 204.
22. Dalgarno, D.; Stehle, T.; Narula, S.; Schelling, P.; van Schravendijk, M. R.; Adams, S.; Andrade, L.; Keats, J.; Ram, M.; Jin, L.; Grossman, T.; MacNeil, I.; Metcalf, C., III; Shakespeare, W.; Wang, Y.; Keenan, T.; Sundaramoorthi, R.; Bohacek, R.; Weigele, M.; Sawyer, T. *Chem. Biol. Drug Des.* **2006**, *67*, 46.
23. Breitenlechner, C. B.; Kairies, N. A.; Honold, K.; Scheiblich, S.; Koll, H.; Greiter, E.; Koch, S.; Schafer, W.; Huber, R.; Engh, R. A. *J. Mol. Biol.* **2005**, *353*, 222.
24. Cowan-Jacob, S. W.; Fendrich, G.; Manley, P. W.; Jahnke, W.; Fabbro, D.; Liebetanz, J.; Meyer, T. *Structure* **2005**, *13*, 861.
25. Ple, P. A.; Green, T. P.; Hennequin, L. F.; Curwen, J.; Fennell, M.; Allen, J.; Lambert-van der Brempt, C.; Costello, G. *J. Med. Chem.* **2004**, *47*, 871.
26. Boschelli, D. H.; Wu, B.; Barrios Sosa, A. C.; Durutlic, H.; Chen, J. J.; Wang, Y.; Golas, J. M.; Lucas, J.; Boschelli, F. *J. Med. Chem.* **2005**, *48*, 3891.
27. Hardcastle, I. R.; Arris, C. E.; Bentley, J.; Boyle, F. T.; Chen, Y. H.; Curtin, N. J.; Endicott, J. A.; Gibson, A. E.; Golding, B. T.; Griffin, R. J.; Jewsbury, P.; Menyerol, J.; Mesguiche, V.; Newell, D. R.; Noble, M. E. M.; Pratt, D. J.; Wang, L. Z.; Whitfield, H. J. *J. Med. Chem.* **2004**, *47*, 3710.
28. Hennequin, L. F.; Stokes, E. S.; Thomas, A. P.; Johnstone, C.; Plé, P. A.; Ogilvie, D. J.; Dukes, M.; Wedge, S. R.; Kendrew, J.; Curwen, J. O. *J. Med. Chem.* **2002**, *45*, 1300.
29. INSIGHT II, 97 Molecular Modelling Program Package; Accelrys, San Diego, CA, 1997.
30. AMRI; www.amriglobal.com, Asinex; www.asinex.com, Enamine; www.enamine.net, InterBioScreen; www.ibscreen.com, Life Chemicals; www.lifechemicals.com.
31. Boehm, H.-J.; Stahl, M.. In *Reviews in Computational Chemistry*; Wiley-VCH: New York, 2002; Vol. 18, pp 41–87.
32. Lipinski, C. A.; Lombardo, F.; Dominy, B. W.; Feeney, P. J. *Adv. Drug Delivery Rev.* **1997**, *23*, 3.
33. Krovat, E. M.; Langer, T. *J. Chem. Inf. Comput. Sci.* **2004**, *44*, 1123.
34. Bissantz, C.; Folkers, G.; Rognan, D. *J. Med. Chem.* **2000**, *43*, 4759.
35. Wang, R.; Lu, Y.; Wang, S. *J. Med. Chem.* **2003**, *46*, 2287.